WIND ENERGY
Wind Energ. (2009)
Published online in Wiley Interscience
(www.interscience.wiley.com) DOI: 10.1002/we.318

Extreme Winds from the NCEP/NCAR Reanalysis Data

Xiaoli Guo Larsén* and **Jakob Mann,** Wind Energy Department, Risø National Laboratory for Sustainable Energy, Technical University of Denmark, Roskilde, Denmark

Key words:
NCEP/NCAR reanalysis data; extreme wind; the 50 year wind; standard conditions

In this study, we test a method to estimate the extreme winds by using the NCEP/NCAR reanalysis data. From the reanalysis pressure or geopotential height records, the geostrophic wind is first calculated, and then extrapolated to 10 m height over a homogeneous surface with roughness length of 0.05 m, i.e. the so-called standard wind. The software Wind Analysis and Application Program will then use this standard wind in a flow model, with the roughness, orography and obstacles around the turbine site to obtain the site-specific wind. The 'annual maximum method' is used to calculate the 50 year wind. We examined extreme winds in different places where the strongest wind events are weather phenomena of different scales, including the mid-latitude lows in Denmark, channelling winds in the Gulf of Suez, typhoons in the western North Pacific, cyclones in the Caribbean Sea, local strong winds: the Mistral in the Gulf of Lions and the Bora in the north Adriatic Sea. It was found that the method introduced here can be applied to places where the extreme wind events are synoptic weather phenomena like in north-western Europe, but a more complicated downscaling, e.g. based on a mesoscale model, is needed for places where the extreme wind events are of mesoscale origin. Copyright © 2009 John Wiley & Sons, Ltd.

Received 14 March 2008; Revised 9 December 2008; Accepted 9 December 2008

Introduction

Reliable estimation of extreme wind is important for wind turbine developers. For each wind turbine site, the most likely extreme wind has to be estimated in order to make sure that the winds will not exceed the turbine's design specification. This is codified by the International Electrotechnical Commission.[1] There is no single, consistent definition of the design wind speed in the field of wind engineering. We choose the definition as used in the European Wind Load Code (Eurocode).[2] It is defined in terms of the 50 year wind, i.e. the 10 min average wind, which, on average, is exceeded once in 50 years. The 50 year wind is based on the so-called *standard wind*, i.e. wind at 10 m, over a flat area with a homogeneous roughness length of 0.05 m. We denote it as U_{50}.

For Europe, the need for a new extreme wind atlas is apparent when looking at the existing Eurocode. Many European countries have made their own extreme wind atlas, e.g. Denmark, France, Germany and the UK.[3–6] However, the procedures used by different countries are not consistent, leading to significant discontinuities in the extreme wind values at national borders. For instance, U_{50} is 24 m s^{-1} in southern Denmark but 32 m s^{-1}

*Correspondence to: X. G. Larsén, Wind Energy Department, Risø National Laboratory for Sustainable Energy, Technical University of Denmark, Building 118, Roskilde 4000, Denmark.
E-mail: xiaoli.guo.larsen@risoe.dk

in northern Germany. This is a significant and unrealistic difference, considering that the loads (and in some cases, also the price of the structure) increase as the square of the wind speeds. This issue has also been addressed by Miller.[7]

The most common problem in obtaining U_{50} for a turbine site is that there are no long-term continuous measurements of reliable quality available. This problem urges people to look for all possible kinds of data sources. The reanalysis data from different global climate models have attracted many because of their spatial and temporal coverage, i.e. globally and in decades. The National Centers for Environmental Prediction/ National Center for Atmospheric Research (NCEP/NCAR)[8] and the European Center for Medium-Range Weather Forecasting (ECMWF) reanalysis data have been of great interest in the past several years to the wind energy industry.

Therefore, we think it is urgent to examine the following issues: What does the global reanalysis data provide? How can we extract useful information out of the reanalysis data and how shall we translate the information for practical use?

In this study, we investigate whether the NCEP/NCAR reanalysis data can be used for extreme wind estimation. We focus on the method by which the geostrophic wind at sea level G_{sl} is first derived from the pressure and temperature records, and is then corrected to the standard wind. Afterwards, the software Wind Analysis and Application Program (WAsP Engineering) from Risø DTU,[9] (http://www.waspengineering.dk) will model the flow over the domain of interest, with detailed description of terrain, roughness and obstacles, and thus transform the standard wind into a realistic wind for the turbine site.

The NCEP/NCAR reanalysis data are thus downscaled directly to micro-scale without the use of a mesoscale model. An uncertainty is introduced through the assumption that the geostrophic wind at the actual wind turbine location is the same as the uniform geostrophic wind over the appropriate grid box in the reanalysis data. Such a grid box is approximately 200 by 200 km, and in practice, mesoscale effects could be significant. In this paper, we will validate the extreme wind estimation from the NCEP/NCAR reanalysis data with wind observations from mid-latitudes as well as from the Gulf of Suez.

The idea of using pressure records to calculate U_{50} was suggested by Davenport in 1963. Lately, Frank[10] applied this method to Denmark, and Miller[7] applied it over the UK and many other places in Europe. They found the results promising, comparing well to observations. Here, since the reanalysis pressures and geopotential heights are available globally, we examine the applicability of this method in different regions where extreme winds are caused by different weather phenomena.

The details of the WAsP Engineering technique are described in the next section. The assumptions used in this linearized micro-scale model include neutrality of the atmospheric stratification and constancy of the geostrophic wind over the modelled domain. Section 3 is devoted to the NCEP/NCAR reanalysis data. In section 3.1, we consider what parts of the almost 60 year long reanalysis time series to use. The first decades assimilated a limited amount of meteorological observations, and some of those were erroneous. Therefore, we only use the most recent two and a half decades. In section 3.2, the critical issue of spatial and temporal resolution is exposed. A too coarse resolution might underestimate the extremes. Finally, in sections 3.3 and 3.4, we display the methods of calculating the geostrophic and the gradient winds, and how to calculate pressures at the same geopotential heights. The details of these matters are essential for obtaining reasonable extreme winds. The method to obtain the 50 year wind from a limited record of data is described in section 4. Because our times series are relatively long, we can safely use standard methods, and those are applied both to the mast observations and the reanalysis data. The results in section 5 are focused on different geographical areas with the intent to show that the success of application of the reanalysis data is very dependent on the local conditions. In northern Europe, where mid-latitude lows dominate, the predictions of the 50 year wind are very reasonable (section 5.1). In some other areas of the world, the extremes are smoothed out, resulting in lower 50 year winds. This can happen in mountainous areas (section 5.2 and 5.3) or in hurricane-prone areas, where the inner parts of the low are poorly resolved (section 5.4). For these reasons, we suggest in the discussions and conclusion (sections 6 and 7, respectively) that clever application of mesoscale modelling is a way to improve predictions.

The description of the key variables can be found in Table I.

DOI: 10.1002/we

Table I. Nomenclature

Variable	Description
P_s	The surface pressure
P_{msl}	The mean sea level pressure, obtained with the 'Shuell reduction' method
P_0	The pressure at mean sea level, calculated from P_s with equation (5)
T_{2m}	Temperature at 2 m
T_0	Temperature at mean sea level, calculated from temperature at elevation h with the standard lapse rate γ
T_m	The average temperature of the fictitious air column between the Earth surface and sea level
u_{10}	The wind speed at 10 m
$u_{0,z}$	The wind speed at height z
u_z	The flat terrain wind speed at height z, corrected from $u_{0,z}$
u_*	The friction velocity
G_{sl}	The geostrophic wind at sea level
u_g, v_g	Two components of G_{sl}
G_{gr}	The gradient wind
u_{st}	The wind speed at standard conditions, here at 10 m, over homogeneous surface with roughness length $z_0 = 0.05$ m
U_T	The T year return wind
U_{50}	The 50 year return wind

The WAsP Engineering Technique

Developers need to transfer the wind information from a measuring site to the turbine site. The widely used software WAsP[11] (http://www.wasp.dk), developed at Risø National Laboratory in Denmark, is designed for this purpose, emphasizing wind resource assessment. The accompanying program WAsP Engineering[9] is designed for the estimation of extreme winds and turbulence. For flat, homogeneous terrains, it is consistent with the conversion factors of the 50 year wind for different roughness classes appearing in many building codes. It is extended to non-simple terrains, as in the European Wind Atlas.[12] The technique has been applied to extreme wind studies and is discussed in depth in Abild and Nielsen; Abild *et al.*; and Abild[13–15] (see also other references[3–10]).

When applying observations to a nearby wind farm site, the observation has to go through the technique in two steps: 'cleaning' (step 1) and 'geostrophic mapping' (step 2). At step 1, we calculate the geostrophic wind from the surface wind at the measuring site using the geostrophic drag law. Firstly, the speed-ups due to orography and roughness should be cleaned out from the wind speed at height z (m), $u_{0,z}$, the flat homogeneous terrain wind speed u_z can be obtained from $u_z = u_{0,z}/[(1 + s_o)\,(1 + s_r)]$, where s_o and s_r are speed-up coefficients due to orography and roughness change, respectively. The surface friction velocity, u_*, is then determined from u_z and the area-averaged surface roughness length, z_0:

$$u_* = \frac{\kappa \cdot u_z}{\ln\left(z \big/ z_0\right)} \tag{1}$$

where $\kappa = 0.4$ is the von Kármán constant. Under extreme wind conditions, neutral stratification is a reasonable approximation. A geostrophic wind, G, can then be calculated from u_* by using the geostrophic drag law (e.g. Tennekes[16]):

$$G = \frac{u_*}{\kappa}\sqrt{\left(\ln\frac{u_*}{fz_0} - A\right)^2 + B^2} \tag{2}$$

DOI: 10.1002/we

where f is the Coriolis parameter, and A and B are dimensionless parameters. Numerous studies in the literature have estimated the values of the dimensionless parameters A and B.[3,7,16,17] The magnitudes of A and B are functions of stability. But in our case, i.e. during neutral conditions, we use the neutral values of Landberg *et al.*,[11] $A = 1.8$ and $B = 4.5$.

At step 2, we assume that the geostrophic forcings over the measuring site and the turbine site are the same. This assumption is reasonable if the two places are not too far from each other. Once again, we use the drag law [equation (2)], now with a new roughness length 0.05 m, to obtain a new friction velocity by iteration. With the new roughness length and friction velocity, the *standard wind*, u_{st}, is now obtained by using equation (1) again.

WAsP Engineering can now transform u_{st} into realistic wind for the turbine site. Note that over the whole model domain, there is no variation of G, and hence u_{st}. The two steps are applied to the point wind observations (see Section 5).

For reanalysis winds, the speed is spatially averaged over the entire grid box. Inside the box, the actual surface conditions (obstacles, roughness and topography) at one place may differ from another site, corresponding to different wind climates, unless the box is entirely over water. Even for data validation, it is pointless to compare directly the reanalysis value with the wind measurements at any site in the area if the surface conditions are not homogeneous.

Instead, we have two options to obtain u_{st} over one grid box. One is to transform the modelled 10 m wind to the standard conditions. In this case, we need the local roughness length, the change in roughness upstream and finally, orography. For this purpose, Frank[10] used the roughness length from the Simple Biosphere (SiB) Model of Dorman and Sellers,[18] which is used by the NCEP/NCAR reanalysis. He found that the surface roughness from the SiB model is too high for Denmark and southern Sweden, and accordingly, the standard wind is significantly overestimated; in northern Germany, where the roughness from the SiB model is rather low, the standard wind from the reanalysis was found to be more reasonable. Quite often, the roughness from the SiB model is unrealistic. The SiB roughness includes the effect of gravity wave drag over complex terrains. Over water grid boxes, the surface can be considered homogeneous, and the roughness length can be obtained from the Charnock formula. Therefore, we believe that the transformation of the surface wind over water is more reliable. However, at the spatial resolution of the NCEP/NCAR, some coastal regions and small islands are treated as water, thus the roughnesses there are smaller than in reality, and consequently, u_{st} will be underestimated. In short, the roughness length for land grid points used in the NCEP/NCAR reanalysis cannot be used to transform the modelled 10 m wind to u_{st}. Unless better sources of the roughness length are available, the option of using the modelled 10 m wind to calculate the 50 year wind should be dropped.

The other option, which we pursue here, is to derive the geostrophic wind directly from the reanalysis pressures or geopotential heights and transform it to the standard conditions directly. Thus, the input of roughness is avoided in the calculation and no correction for the orography is needed before u_{st} is obtained.

In section 3.3, the derivation of the geostrophic wind G with the NCEP/NCAR pressure data is given, and the algorithm for reducing the surface pressure (P_s) to the mean sea level and discussions about the limitations of the reduction can be found in section 3.4.

The NCEP/NCAR Reanalysis Data

Data Status

The NCEP/NCAR reanalysis data are available back to 1948. As documented in Kistler *et al.*,[19] although the reanalysis data assimilation system is maintained constantly, the observing system used in the assimilation has evolved in three major phases: 1948–1957, when the first upper-air observations were established; 1958–1978, the modern global rawinsonde network was introduced; and 1979–present, the modern satellite era. During the first decade (1948–1957), the upper-air observations were few and primarily in the northern hemisphere. Some studies, e.g. Bromwich and Fogt,[20] found that the pressure data quality is much improved in the last era.

DOI: 10.1002/we

In 1973, a new scheme of encoding rawinsonde data was introduced, enabling better quality control, more efficient error detection and correction.

According to Kistler *et al.*,[19] there were three human errors made in the assimilation, which were discovered too late to repeat the period of reanalysis affected by the error. These errors are listed here in Table II.

One of the errors is that the snow cover field from 1973 was mistakenly used for the period 1974–1994. This spoils the reliability of the temperature at 2 m, T_{2m}, which is related to the skin temperature in regions where the snow cover differs from 1973. T_{2m} in our calculation directly affects the reduction of pressure to sea level. As will be described in section 3.4, in the 'Shuell reduction' algorithm used by NCEP, the mean sea level pressure P_{msl} is not affected by T_{2m}. However, the slight difference between extreme winds from the P_s and those from P_{msl} suggests that these errors are not significant.

In the reading of Australian P_s data, the use of a different convention for longitude led to a shift of 180º in the use of data for 1979–1992. Investigation of this problem shows that the impact of this error is small and only the southern hemisphere mid-latitude (40º–60º *S*) is affected considerably.[19] However, the Australian P_s data were not used in the reanalysis of the ECMWF. So using ECWMF reanalysis would provide a good alternative for the southern hemisphere mid-latitude.

Also listed in Table II is the problem with the encoding of surface- and sea-level pressures for the period 1948–1967, which resulted in rejected pressure observations in the vicinity of extratropical cyclones, especially for Europe (see http://www.emc.ncep.noaa.gov/gmb/bkistler/psfc/psfc.html). Since this issue is directly related to extreme wind events, we reject the data from 1948–1967 to avoid this problem.

Because of the facts listed above, and in order to keep the data quality consistent, we choose to use the data in the third era, 1979–2005, to calculate the 50 year wind. According to Harris,[21] the uncertainty in estimating the 50 year wind by using 27 year data is about 2–6%, only slightly larger than that by using a data length of 50 years, which is 1–4%.

Data Resolution

The NCEP/NCAR 10 m wind (u_{10}), P_s and temperature at 2 m (T_{2m}), are archived in Gaussian grids with a longitudinal resolution 1.875º and a meridional resolution of approximately 1.904º. The records of the mean sea level pressure P_{msl} and geopotential heights Φ are archived in grids of a resolution 2.5º × 2.5º.

The observations are assimilated every 6 h. As a matter of convention, the European standard and the World Meteorological Organization base the definition of the 50 year wind on 10 min averages. In our earlier paper,[22] we studied the effects of disjunct sampling intervals on the annual wind maximum. There, we developed theoretical and empirical models to estimate the reduction of the extreme wind for sampling intervals as well as averaging times longer than 10 min. We assume that the six hourly outputs of the reanalysis data can be treated as data with a disjunct sampling interval of 6 hours.

Table II. Data status for NCEP/NCAR reanalysis variables P_s, T_{2m}, P_{msl}

Variable	Period	Status
P_s	1948–1967	Problems in the encoding
T_{2m}	1974–1994	The snow cover field for 1973 was used for this period. T_{2m} is affected accordingly.
P_{msl}	1948–1967	Problems in the encoding
	1979–1992	The Australian Ps data were not read correctly, which affected southern hemisphere mid-latitude, ~40º–60º

DOI: 10.1002/we

The Geostrophic Wind

The geostrophic wind is calculated under the assumption of a balance between the pressure gradient and the Coriolis force. It is calculated using the NCEP/NCAR reanalysis data from five, four or three grid points.

When using five grid points, the components of the geostrophic wind at sea level, u_g and v_g, are calculated with pressure gradients, which are calculated as mean sea level pressure differences $\Delta P_{0,j}$ over $2\Delta\varphi$ and $\Delta P_{0,i}$ over $2\Delta\lambda$:

$$u_g = -\frac{1}{f\rho}\frac{\Delta P_{0,j}}{2r\Delta\phi},\ v_g = \frac{1}{f\rho}\frac{\Delta P_{0,i}}{2r\Delta\lambda\cos\phi} \tag{3}$$

where r is the Earth radius and ρ is the air density. The latitude difference $\Delta\varphi = \varphi_{j+1} - \varphi_j$ and longitude difference $\Delta\lambda = \lambda_{i+1} - \lambda_i$ are in radians. The air density is calculated through $\rho = P_{0,ij}/(RT_{0,ij})$, where R is the gas constant for dry air, and $P_{0,ij}$ and $T_{0,ij}$ are the pressure and temperature at mean sea level at grid (i,j). The geostrophic wind speed is denoted by $G_{sl} = (u_g^2 + v_g^2)$. In the current paper, unless otherwise stated, G_{sl} is calculated with equation (3), with five grid points used.

As also pointed out by Miller,[7] by using mean sea level pressure in equation (3), strictly speaking, we are not calculating the wind at the top of the boundary layer. However, it was found to be a good approximation suggested by the radiosonde measurements given in Watson *et al.*[23]

For the calculation in this paper, we use r = 6,370,997 m, which is the radius of the earth at mid-latitudes in spherical coordinates. Traditionally, in describing the atmospheric movement with which meteorologists are concerned, a constant earth radius is used.[24] When obtaining the NCEP/NCAR reanalysis data, a constant gravitational acceleration is used globally. An estimation of the difference in the geostrophic wind was made here, treating the Earth as an ellipsoid instead, with r varying with latitude. The difference was found to be at most 0.5%.

Equation (3) does not apply in the tropical regions where $f \sim 0$.

When using four grid points, the values of P_0 and T_0 at $\left(i-\frac{1}{2}, j\right)$, $\left(i-\frac{1}{2}, j-1\right)$, $\left(i-1, j-\frac{1}{2}\right)$, $\left(i, j-\frac{1}{2}\right)$ and $\left(i-\frac{1}{2}, j-\frac{1}{2}\right)$ are first interpolated from the four circled grid points, and then the above equation is applied with the pressure gradient over $\Delta\varphi$ and $\Delta\lambda$, thus (u_g, v_g) at $\left(i-\frac{1}{2}, j-\frac{1}{2}\right)$ are obtained. With this method, $\rho = P_{0,i-\frac{1}{2},j-\frac{1}{2}} \Big/ \left(RT_{0,i-\frac{1}{2},j-\frac{1}{2}}\right)$.

There are two ways to calculate G_{sl} using three grid points for the centre point of a triangle.

For an irregular triangle, one can follow the algorithm described in Kristensen and Jensen.[25] For a triangle with a right angle, the pressure difference is calculated over $\Delta\varphi$ and $\Delta\lambda$, and $\rho = P_{0,i-\frac{2}{3},j-\frac{2}{3}} \Big/ \left(RT_{0,i-\frac{2}{3},j-\frac{2}{3}}\right)$, where P_0 and T_0 at $\left(i-\frac{2}{3}, j-\frac{2}{3}\right)$ are linearly interpolated. Other combinations using three of the four points in a grid box give the other three centre points.

The final estimate of the extreme wind is not sensitive to which method is used, namely, using five, four or three grid points, to calculate G_{sl}. They give consistent results and the difference is normally in the range of 0 to ± 1 m s^{-1}.

When the site of interest is experiencing a strong cyclonic condition, the assumption of the balance between the pressure gradient and the Coriolis force [equation (3)] will overestimate the wind aloft, because the acceleration G_{gr}^2/l may play an important role:

$$G_{sl} = G_{gr} + G_{gr}^2/(lf) \tag{4}$$

DOI: 10.1002/we

where l is the radius of curvature of the isobars and G_{gr} is the gradient wind.[24] According to the above equation, the effect of isobar curvature, $G_{gr}^2/(lf)$, is large at small f (i.e. in the tropics, but not too close to the equator where there is no Coriolis force and, therefore, cyclones do not develop), close to the storm centre where l is small and at strong winds, i.e. large G_{gr}. However, this method is not intended to apply in the tropics. Also, at very small l, i.e. very close to the storm centre, the wind is usually rather calm. We calculated l with the second-order pressure differentiation.[25,26] In the northern hemisphere, G_{gr} is less than G_{sl} in cases of cyclonic conditions where $l > 0$. When $l < 0$, the ratio of G_{gr}/G_{sl} is larger than 1 and it increases rapidly towards infinity as the variable $G_{sl}/(fl)$ approaches –0.25. By then, the precision of the data does not reach the demand of the calculation of a second-order differentiation of pressure. Accordingly, artificially high values of G_{gr} can be easily produced by the correction. This would mislead the selection of annual wind maxima, and accordingly, brings a lot of scatter. A comparison of the u_{st}-distribution over all water grid points was made between the values calculated from G_{sl} without the curvature correction and those calculated from the modelled 10 m wind with the Charnock formulation for the roughness length. The general patterns of the two are very similar. However, when $G_{gr}^2/(lf)$ is added, there turns out to be a significant and sporadic difference between the result from the 10 m wind and that from the gradient wind.

Based on these reasons, we proceed with $G = G_{sl} = G_{gr}$ to obtain u_{st}.

Reduction of Pressure to Mean Sea Level

The integration of the hydrostatic equation provides the mathematical basis for the reduction of P_s to the sea level P_0:

$$P_0 = P_s \exp\left(\frac{gh}{RT_m}\right) \tag{5}$$

where g is the gravitational acceleration, h is the elevation and T_m is the average temperature of the fictitious air column between the Earth surface and sea level. Often, the standard atmosphere lapse rate ($\gamma \equiv 0.0065\ \mathrm{km}^{-1}$) is used to extrapolate the temperature at surface T_s to sea level T_0, although the study of Benjamin and Miller[27] suggested that this standard lapse rate was more accurate in spring and autumn, while too stable in summer and too unstable in winter. The average of the temperature at the current time and that of the previous 12 h was used for the current time in the calculation. This was done in order to remove the influence of the diurnal temperature wave on the reduction;[27] however, it only leads to negligible differences in the estimate of the extreme wind.

This method for the pressure reduction works least well over high terrains with a significant elevation gradient, for instance over the Tibet Plateau. There have been many proposals for dealing with this problem, but it remains to be solved, see e.g. Mohr; Pauley.[28,29] In the USA, the 'plateau correction' is used for stations with elevation larger than 305 m above sea level, e.g. Benjamin and Miller; Mohr.[27,28] This correction is made to ensure that, at all stations, the average mean sea level pressure difference between January and July is about 5 hPa, which is typical for stations at the same latitude and longitude in the USA. However, it is not a straightforward procedure to apply to other places without further examination and validation.

The mean sea level pressures P_{msl} from NCEP/NCAR were calculated from the 'Shuell reduction' algorithm in model forecasts and analyses since 1970 at NCEP. They are reasonably comparable to the standard reductions performed at individual stations.[29,30] In this method, T_m is set to be the average of two temperature parameters: one is the 'ground temperature', extrapolated from temperature in the lowest model layer using the standard lapse rate γ; the other one is the 1000 mb temperature, extrapolated from the 'ground temperature' using γ.

Therefore, the method introduced in this paper is not recommended for places with high irregular terrain. For high but flat terrain, the geopotential height Φ at the corresponding elevation level is a better choice than the pressure.

DOI: 10.1002/we

The Annual Maximum Method

We use the annual maximum method to estimate U_{50}. From a record of n years, the annual maximum winds are sorted in ascending order: $U_i^{\max}$, where $i = 1, \ldots, n$. It can be shown that if the tail of wind distribution is exponential, then the extreme winds have an accumulated probability $F(U)$ that is double exponential:[31]

$$F(U) = \exp(-\exp(-\alpha(U-\beta))) \tag{6}$$

In short, we use the Gumbel (Type I) extreme wind distribution to fit a set of annual maximum wind speeds. The probability-weighted moment procedure is applied to obtain the coefficients α and β:[15–32]

$$\alpha = \frac{\ln 2}{2b_1 - \overline{U^{\max}}}, \beta = \overline{U^{\max}} - \frac{\gamma_E}{\alpha} \tag{7}$$

where $\gamma_E \approx 0.577216$ is Euler's constant, $\overline{U^{\max}}$ is the mean of $U_i^{\max}$ and b_1 is calculated from

$$b_1 = \frac{1}{n}\sum_{i=1}^{n}\frac{i-1}{n-1}U_i^{\max} \tag{8}$$

The values of α and β are not very different from those obtained from the least square regression method to $U_i^{\max}$ versus $-\ln\left(-\ln\frac{i}{n+1}\right)$. However, according to Abild[15] and Hosking,[32] this simple method yields less bias and variance on the parameter estimates and has been proven highly efficient even for small size samples. Substituting equation (6) into the relationship between the cumulative probability $F(U)$ and the reoccurrence interval T:

$$T = (1 - F(U_T))^{-1} \tag{9}$$

gives the T year wind speed:

$$U_T = -\alpha^{-1}\ln\ln\frac{T}{T-1} + \beta \approx \alpha^{-1}\ln T + \beta \tag{10}$$

The uncertainty of U_T can be calculated from the uncertainties on α and β, as also given in Mann *et al.*:[33]

$$\sigma(U_T) = \frac{\pi}{\alpha}\sqrt{\frac{1 + 1.14k_T + 1.10k_T^2}{6n}} \tag{11}$$

where

$$k_T = -\frac{\sqrt{6}}{\pi}\left\{\ln\ln\left(\frac{T}{T-1}\right) - \gamma_E\right\} \tag{12}$$

The detailed derivation can be found in several other articles.[15–32] Figure 1 shows an example of the distribution of U_T with T at a Danish site, Tystofte.

For directional cases, we divide the winds in 12 sectors centred at 0º, 30º, 60º, . . . , 330º, and perform the same procedure as for the omnidirectional case to obtain sectorwise 50 year winds.

There are numerous studies on the topic of which distribution function fits best to the complicated extreme wind cases, see e.g. Simiu and Heckert; Holmes and Moriarty; and Palutikof *et al.*[34–36] It is, however, beyond the main intention of this study. The annual maximum method has worked quite satisfactorily in the mid-latitudes, and it is practical for many engineers because of its simplicity. This method deals with extremes of independent identically distributed samples, i.e. the wind speed distribution from each year has the same parent

DOI: 10.1002/we

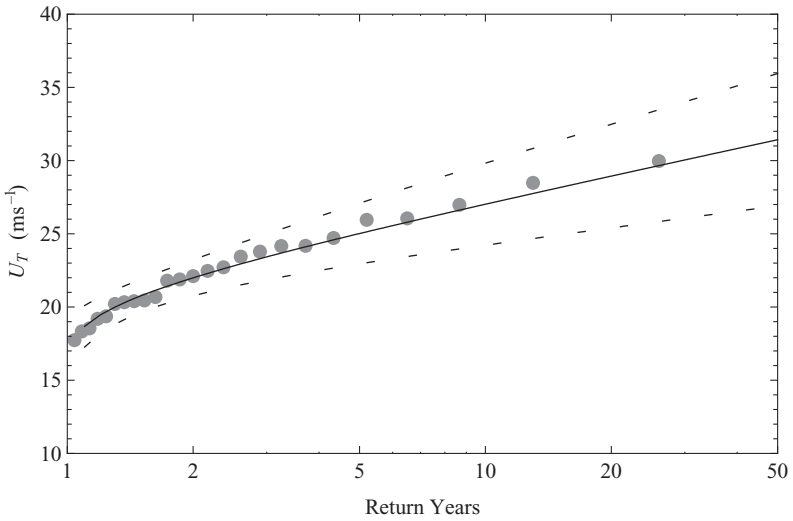

Figure 1. Distribution of U_T *with* T *at a Danish site, Tystofte, based on measurements of 10 min averages at 39.3 m, the solid curve shows the fit of equation (10). The dashed curves show the 95% confidence intervals*

Table III. Information on the wind observations, at four Danish stations as well as two Gulf of Suez stations, including the station positions, the observation heights and data periods

Site	(Latitude, longitude)	Height (m)	Period of observation
Sprogø	(55.3314º, 10.974º)	70	1977–1999
Tystofte	(55.2400º, 11.3300º)	39.3	1982–2006
Kegnæs	(54.8558º, 9.9364º)	23.4	1991–2005
Jylex	(55.9422º, 8.4486º)	24	1982–2004
Abu Darag	(29.2803º, 32.5992º)	24.5	1991–2001
Hurghada	(27.3164º, 33.6989º)	24.5	1991–2001

probability distribution. By this method, all the samples are supposed to be from the same physical dynamics of weather. However, this is not always the reality. At a place where the weather systems are complicated, the extremes may have different meteorological mechanisms. The samples of different mechanisms need to be sorted before being fitted to an appropriate extreme value distribution.[37] Otherwise, the distribution of U_T with T could deviate significantly from the Gumbel prediction.

Results: The Extreme Wind

In the following, some extreme winds at different places, contributed by different weather phenomena of different scales, are examined. We use available long-term wind observations from Denmark and the Gulf of Suez to validate U_{50} from the reanalysis data. The measurements are all 10 min averages, and further information of the wind observations is given in Table III.

Denmark

In Denmark, the weather is dominated by the mid-latitude depressions. In this section, we first use simultaneous and continuous pressure measurements from six stations in Denmark to validate the reanalysis G_{sl}. The

DOI: 10.1002/we

barometers have a long-term accuracy of about 0.1 hPa, which at sea surface, corresponds to the weight per unit area of an air column of about 0.8 m. To match the accuracy, the altitudes of the barometers have been determined to an accuracy better than 0.5 m. The air temperature was also measured and it was used to transform the pressure to the sea level by equation (5) for further calculation of G_{sl}. All measurements are 10 min averages and they cover the period from April 1998 to November 2001. The locations of the stations are given in Figure 2. Ten reasonable combinations of three of the stations were used to calculate G_{sl} at the centre point. They are numbered 0–9 and referred to as Me_i, where $I = 0, \ldots, 9$ (see Figure 2a).

For the reanalysis data, we could obtain G_{sl} from the P_s by equations (5) and (3), or from the mean sea level pressure P_{msl} directly. Based on the arguments given in section 3.4, we focus on the results from P_s, but use those from P_{msl} as a reference.

The shaded numbers 1–24 in Figure 2b are centre points of all combinations of three neighbouring grid points, where the P_s records are available; these centres will be referred to as Re_i. Positions marked with non-shaded numbers are for P_{msl}; because of the slightly more crude resolution of P_{msl} (i.e. 2.5º), only eight triangle centres covering Denmark.

The correlation coefficients of the pressure at sea level, P_0 calculated from P_s with equation (5), G_{sl} and geostrophic wind direction G_{dir}, between measurements and the reanalysis data at the nearby triangle centres (here Re_i) are calculated. Good correlation between the observation and the reanalysis data is found, with the correlation coefficient for P_0 varying between 0.993 to 0.996, for G_{sl} between 0.830 to 0.898 and for $\sin(G_{dir} \cdot \pi/180)$ between 0.942 to 0.953. The spectra of the time series of P_0 as well as G_{sl}, for observations and reanalysis data from their closest grid points, have the same shape and energy density up to the frequency of half day, which is the Nyquist frequency of the reanalysis data (see, an example, Figure 3. The spatial distribution of the monthly mean G_{sl} from the reanalysis data has also shown to be consistent with observations, both in magnitude and direction. This suggests that, for Denmark, the reanalysis data can realistically represent the wind climate in the period from April 1998 to November 2001.

In Figure 4, we show four snapshots of G_{sl} vectors during a severe storm that hit Denmark on 3 December 1999 and caused €1.5 billion worth of damage. In this figure, the observations are 10 min values. At centres (Me_i) where data are missing at that time, no arrows are drawn. The time stamps are given in the titles of each subplot. On top of the observations, we plot as well the G_{sl} vectors of the reanalysis data, at the closest available time stamps, in order to show how storms are described in the reanalysis data in comparison to observations. Considering the wind distribution in both magnitude and direction, the agreement between the

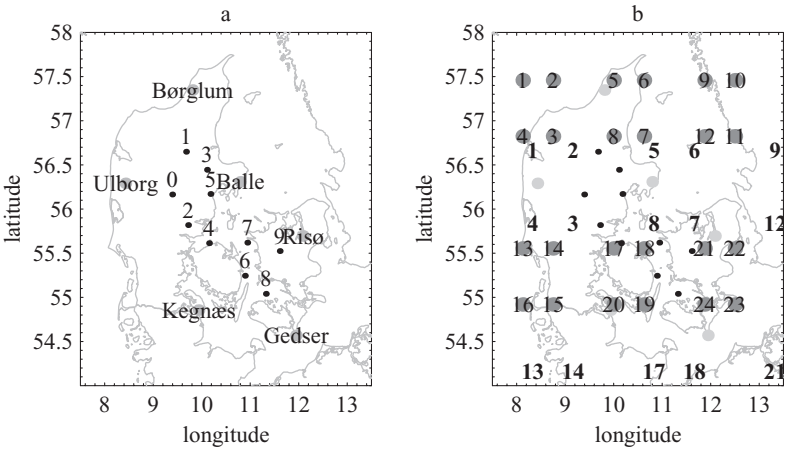

Figure 2. (a). The six stations indicated by the station names and 10 measurement centres $\mathrm{Me_i}$, $\mathrm{i} = 0, \ldots, 9$ *built from the stations, indicated by numbers 0 to 9. (b). Centres of every three neighbouring grid points, shaded numbers are for* $\mathrm{P_s}$, $\mathrm{Re_i}$, $\mathrm{i} = 1, \ldots, 24$; *non-shaded numbers are for* $\mathrm{P_{msl}}$

DOI: 10.1002/we

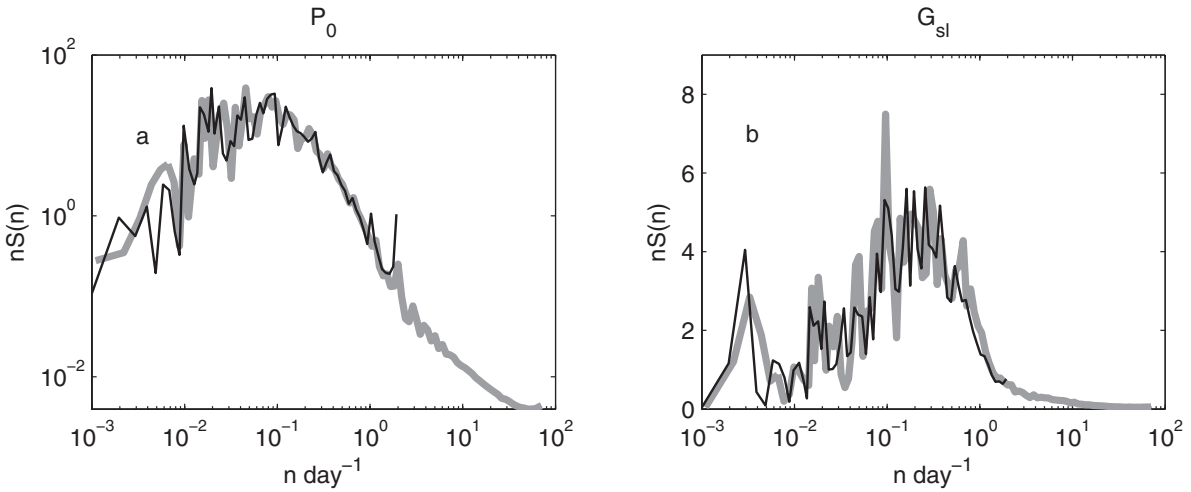

Figure 3. Spectra of P_0 *and* G_{sl} *at* Me_8 *(grey, observation) and* Re_{24} *(black, reanalysis data), n is the frequency and* S(n) *is the energy density*

observations and the reanalysis data is good before and after the storm peak, namely Figure 4(a),(d). At around 18:00, i.e. at the storm peak [see Figure 4(b),(c)], the reanalysis data captured the form of the cyclone, with the storm centre consistent with the satellite picture (http://www.sat.dundee.ac.uk/auth.html), but the winds seem somewhat underestimated.

The omnidirectional U_{50} at the four Danish sites are given in Table IV. For observations, the period given in Table III is used (first column), and for the reanalysis data, both the period 1979–2005 (second column) and that overlaps with the observations are used (last column). Using data of different periods tends to introduce bias to U_{50} if the extreme wind climate changes significantly, especially for short-time series. Here, the difference in U_{50} is at most about 1 m s^{-1} when using the reanalysis data for the entire period and only those overlap with the observations; it is within the range of uncertainty calculated from equation (11). At first glance, the 6 h reanalysis data underestimate U_{50}; however, after correcting to the 10 min values by using a ratio of 0.88 based on Larsén and Mann,[22] the reanalysis data give U_{50} closer to the observations, with differences within the range of uncertainty given by the observations. Note that U_{50} at the Danish sites are not the same as those in Kristensen *et al.*,[3], mainly because of two facts. Firstly, Kristensen *et al.*[3] used shorter time series. Secondly, Kristensen *et al.*[3] used 2 months as the basis period, while here, we use 1 year. Using 2 months introduces low extreme wind speeds during the summer. Accordingly, the wind distribution may differ from that obtained by using 1 year as the basis period. This could violate the preconditions of using the periodic maximum method.

The directional distribution of U_{50} for the four Danish sites are plotted in Figure 5. The reanalysis data successfully found the strong winds in the west sector, although the values are underestimated (see the grey curves). After being corrected roughly to the 10 min values by using a ratio of 0.88, the underestimation is diminished. Considering the uncertainties in the observations, the agreement between the observations and the reanalysis data of about 2 m s^{-1} is acceptable.

Europe

The contour lines of U_{50} over a part of Europe are presented in Figure 6(a). Miller[7] used mean sea level pressure maps over the period 1953–1995 from the archives of the UK Meteorological Office to calculate the geostrophic wind and then the 50 year wind, a method similar to the one we used here. Those pressure maps are available every 6 h. Instead of the Annual Maximum Method, Miller used the 'peak-over-threshold' method

DOI: 10.1002/we

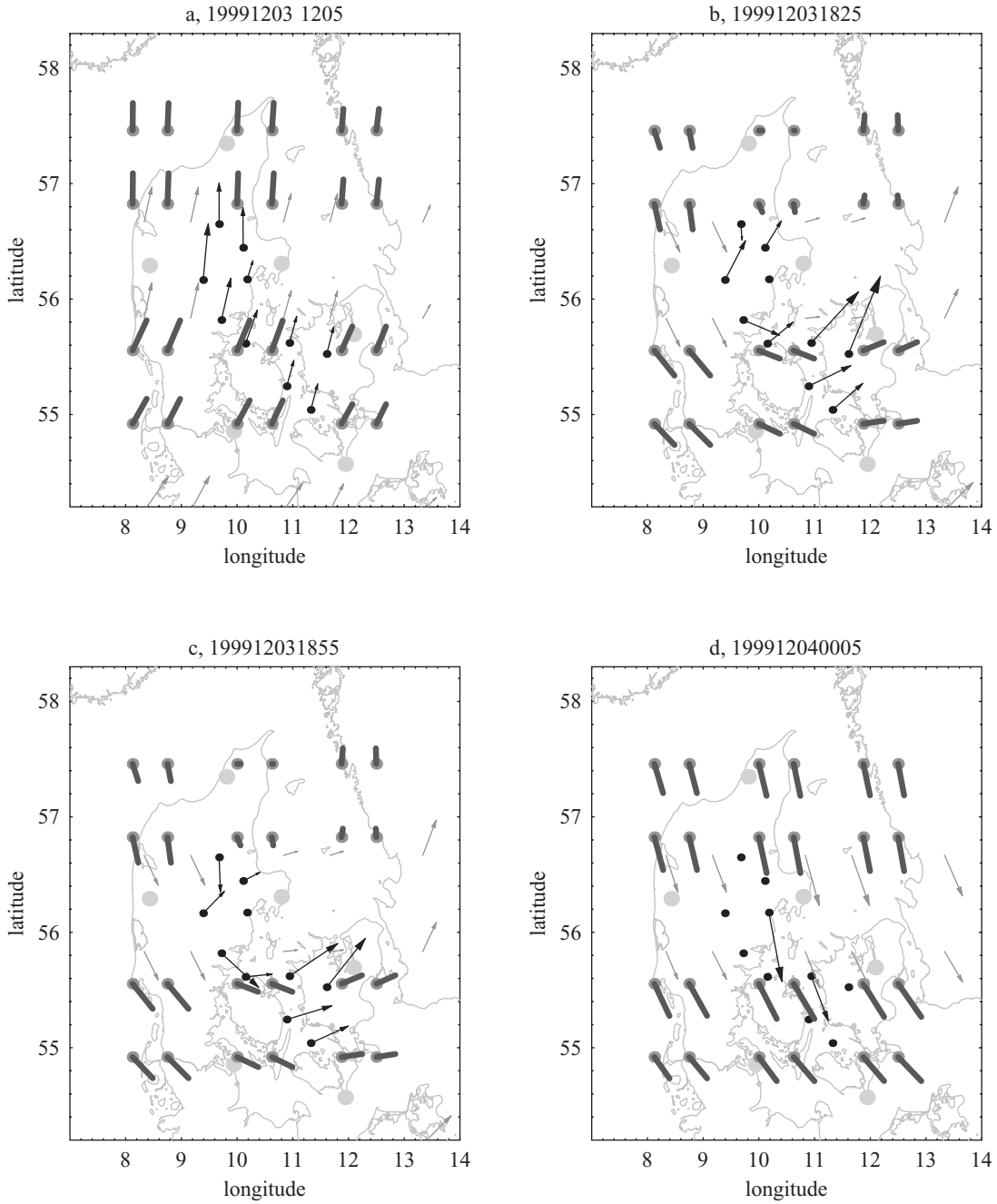

Figure 4. Snapshots of G_{sl} *m s*$^{-1}$. *Black arrows at* Me_i *are measurements at the time as indicated in the plot titles, thick grey arrows at* Re_i *are calculated from reanalysis data (*P_0*) at the closest available time stamps to the observation, and the thin grey arrows are calculated from reanalysis data* P_{msl}. *The scale for arrows is the same in the four plots; in (a) at* Me_1, G_{sl} *is 25 m s*$^{-1}$

DOI: 10.1002/we

Table IV. The omnidirectional 50 year wind, from observations: $U_{50} \pm$ uncertainty (m s^{-1}), from reanalysis data 1979–2005 and from reanalysis data overlapping with the observations: $U_{50,6h}$ ($U_{50,10\,\mathrm{min}}$). The numbers in brackets are the corrected 10 min values by using a ratio of 0.88 (1/1.14) to the 6 h values. The uncertainty of U_{50} from the observations was calculated according to Mann *et al.*[33]

Site	Observation	NCEP/NCAR (1979–2005)	NCEP/NCAR (overlapping with observation)
Sprogø	23.9 ± 2.0	22.9 (26.0)	22.5 (25.7)
Tystofte	25.7 ± 2.9	22.9 (26.0)	23.5 (26.8)
Kegnæs	26.3 ± 3.8	22.5 (25.6)	21.4 (24.4)
Jylex	29.1 ± 2.9	23.9 (27.1)	22.8 (26.0)
Abu Darag	20.0 ± 2.1	14.4 (16.4)	14.9 (17.0)
Hurghada	15.1 ± 0.9	13.3 (15.1)	13.0 (14.8)

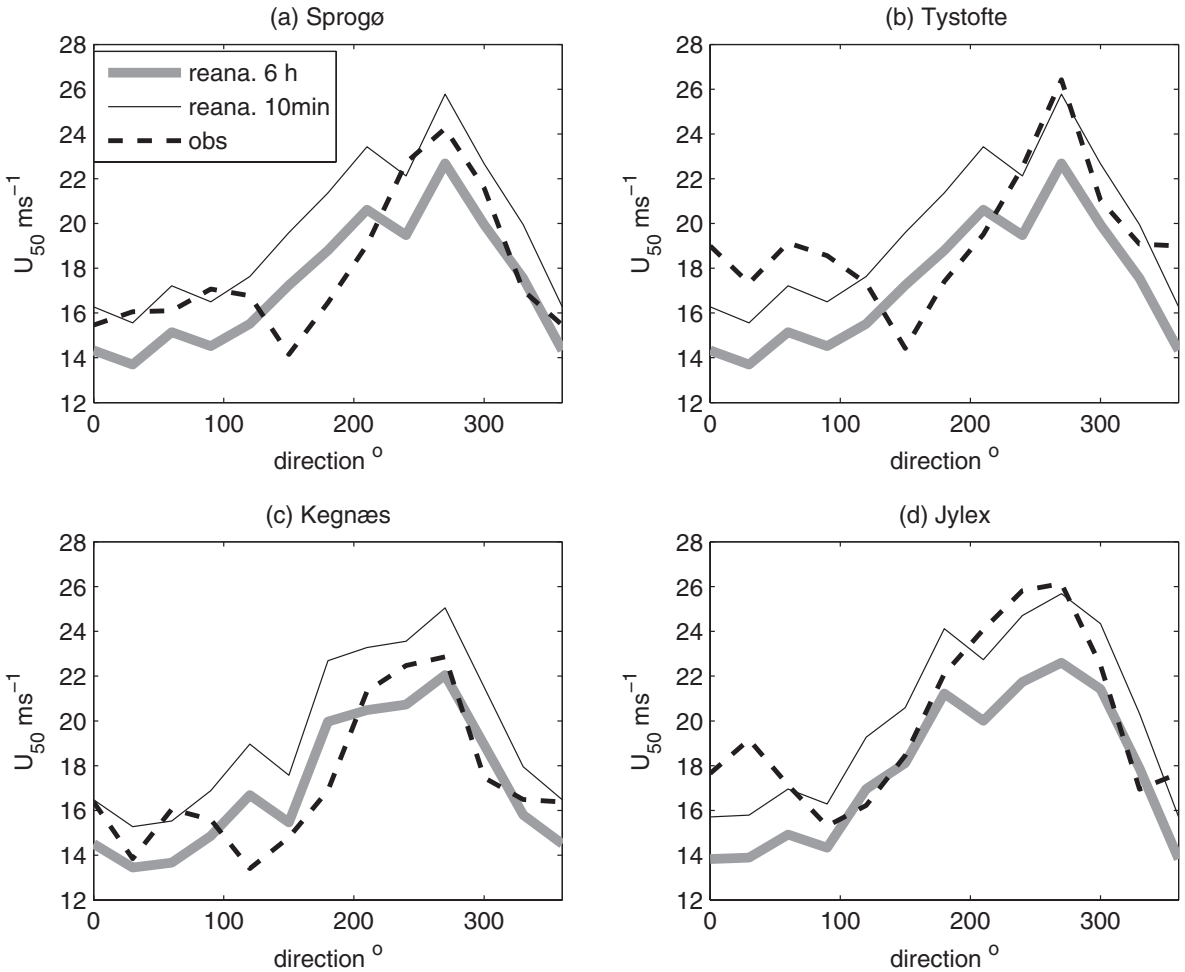

Figure 5. Directional distribution of U_{50} at four Danish sites. The thick dashed curves are from 10 min observations, the thick grey curves are 6 h values from the reanalysis data and the thin solid curves are 10 min reanalysis values corrected from the 6 h values by using a ratio of 0.88

DOI: 10.1002/we

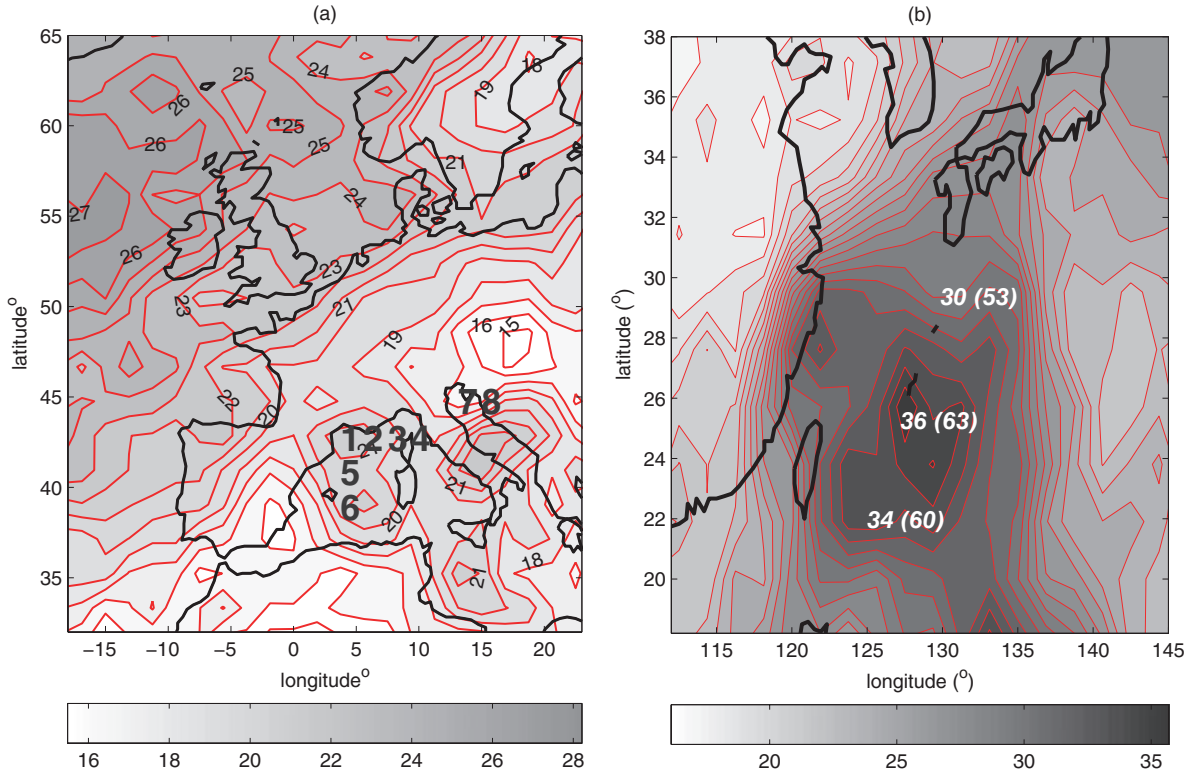

Figure 6. Distribution of U_{50} m s^{-1} from the NCEP/NCAR reanalysis data 1979–2005. The contour lines represent the 6 h values. (a) Part of Europe. The bold numbers mark the grid points for studying the Mistral (1–6) and the Bora (7–8). (b) Western North Pacific. The numbers in the brackets are corrected from the 6 h values (those outside of the brackets) to be 3 s gust values over roughness length of 0.03 m

described by Holmes and Moriarty.[35] Miller also derived the values of A and B for equation (2) as 1.40 and 5.79, respectively, which, for a given G, will give systematically slightly smaller u_* and accordingly smaller u_{st}, and eventually, smaller U_{50}. These facts explain partly the differences between his final plot of U_{50} (figure 5 in his paper) and our current plot. Nevertheless, his result turns out to be similar to our Figure 6(a). Over the common domain, namely, (15ºW–15ºE, 42.5ºN–62.5ºN), U_{50} decreases generally from north-west to south-east, with a hot spot extending from the North Sea to northern Germany, where the magnitudes of U_{50} in both figures are comparable.

In Europe, the Mistral and the Bora are two types of local strong winds. The Mistral blows north-westerly from south France into the Gulf of Lions. It is strongest in the Gulf but can extend beyond Sicily into the eastern part of the Mediterranean basin. Six grid points, numbered 1–6 in Figure 6(a), are chosen to study the Mistral. We see a hot spot in the Gulf of Lions. At point 1, 85% of the time, the yearly strongest wind is in the west to north sector 300º–10º. From this sector, the wind frequency decreases to 81% at point 2, 63% at point 3 and 30% at point 4. To the south, at points 5 and 6, the wind frequencies from this sector are 93% and 70%. This indicates weakening Mistral impact away from the Gulf of Lions. At points 1, 2 and 5, the strongest winds occur mostly from October to March, which is the typical period for the Mistral but also the period to have the deepest mid-latitude depressions. It is very likely that the yearly maxima come from both phenomena.

Cold air accumulates over Yugoslavia, spills over high mountain passes and reaches the North Adriatic Sea as a strong wind, the Bora. Only two grid points cover the area: points 7 and 8 in Figure 6(a), with one water

DOI: 10.1002/we

grid and one land grid. The typical direction for the Bora is north-easterly, and it occurs mainly in winter. In the sector 350º–60º, the wind frequency is 93% at point 7 and 85% at point 8. For more than 83% of the time, the yearly strongest winds occur from November to February. The wind direction and seasoning of the strongest winds match the characteristics of the Bora in this region.

However, although the general characteristics of the two katabatic winds seem to have been captured, the model resolution is too crude, leading to the local winds smoothed out, resulting in rather low extreme winds here.

The Gulf of Suez

Abu Darag is located on the coast of the northern part of the Gulf of Suez (see the map in Larsén and Mann[22]). The channelling wind contributes to the extreme wind.

Leaving the Gulf of Suez and entering the Red Sea, the wind climate changes significantly. Hurghada is located in the southern part of the Gulf, bordering the Red Sea. There is a distinct seasonal variation in wind direction while the seasonal variation in wind speed is rather weak. In spring and summer, the strongest wind is mostly from north–north-west because of the channelling effect; in autumn, it is from the west-to-north sector and in winter, it is from the west because of synoptical pressure gradient. The strongest winds from the two mechanisms do not differ significantly in magnitude, and the extreme winds could come from both.

The omnidirectional U_{50} at the two sites are given in Table IV. At Abu Darag, the reanalysis data considerably underestimated the extreme winds while giving almost the same value as the observations at Hurghada. It is not unexpected that the reanalysis missed the mesoscale channelling winds at Abu Darag. First, the width of the channel is about 50 km and it is hardly resolved by the reanalysis data resolution of about 200 km. Second, the mesoscale study of Badger *et al.*[38] suggests, to a similar case, that the local topographical channelling effect can become detached from the background geostrophic wind but depends on the Froude number. The good estimate at Hurghada seems to be a coincidence: the background pressure gradient winds that are captured in the reanalysis data happen to be of the same magnitude as the channelling winds.

Tropical Cyclones in the Western North Pacific and the Caribbean

In the western North Pacific Ocean, typhoons are generated frequently. They move north-westwards, often over The Philippines and Taiwan, then turn north-eastwards. In this region, the typhoons are responsible for the extreme winds. With the typhoon track data from the Japanese Meteorological Agency as used in Ott,[39] we find that, for severe individual typhoons, the NCEP/NCAR centre low pressure can accurately reproduce the typhoon tracks, but weak typhoons are sometimes not seen in the pressure record. However, in general, the strongest typhoons in this region, which are mainly responsible for the extremes, are of a size larger than the reanalysis resolution. So, the problem is not that all typhoons are not resolved but the spatial smoothing and crude temporal resolution of the severe typhoons.

Ott[39] used the typhoon track data from 1977 to 2004 and the so-called Dvorak method to correlate certain features of storm images with measures of storm intensity, calculate the geostrophic winds and finally to estimate the 50 year wind.

In Figure 6(b), U_{50} from the NCEP/NCAR data is presented and some contour lines are marked with the corresponding values. The three numbers in the brackets are 3 s gust values over the roughness length of 0.03 m. This was done to make comparison with Ott's results, which are 3 s gust values over 0.03 m roughness. In obtaining the gust values, again, we correct roughly the 6 h values a ratio of 0.88[22] to obtain the 10 min values, and then apply gust factor 1.4, which is typical for the mid-latitude.

The comparison indicates that the reanalysis data predict the strongest winds a few degrees north of the area indicated by the storm track data. The hot spot in Ott's plot is ~75 m s^{-1}, while the reanalysis data give ~63 m s^{-1}. The underestimation by the reanalysis data is obvious, although the uncertainties in the storm track data analysis may also be responsible for the difference.

DOI: 10.1002/we

In the Caribbean Sea, the cyclone sizes are generally small so that they are mostly not resolved by the reanalysis data; even strong cyclones are sometimes not seen in the reanalysis pressure data. Therefore, the extreme winds in this region are significantly underestimated.

Discussions

This study was based on the earlier work of Frank for Denmark on using the reanalysis pressure data to obtain u_{st}.[10] Use of the pressure data to obtain u_{st} has also been shown to be a promising method in the study of Miller[7] for Europe. In the standard WAsP/WAsP Engineering code, the observations from a nearby site to the turbine site are cleaned from the local effects of roughness, orography and obstacles to obtain G_{sl}, which is assumed to be the same as that over the turbine site. Here, we assume that G_{sl} is the same over the reanalysis data resolution, i.e. ~200 km, which is larger than assumed in WAsP Engineering. This introduces spatial smoothing, which could increase the uncertainty of the extreme wind calculations.

Data validation is therefore needed. The point measurements are from Denmark and the Gulf of Suez. In Denmark, the extreme winds are due to the synoptical mid-latitude depression, while in the Gulf of Suez site Abu Darag, it is the mesoscale channelling winds that contribute to the extreme winds. At the other Gulf of Suez site, both the synoptical pressure gradient and the channelling winds can give extreme winds.

Comparisons with measurements from Denmark show that the reanalysis data captured the mean wind characteristics well. Indeed, the reanalysis data were seen to give the correct position and form of one of the most severe storms that has hit Denmark. With the time resolution effect corrected by the method given in our earlier study[22] where the wind time series was assumed to behave like a Gaussian Markov chain, the extreme winds from the reanalysis data at the Danish sites are in good agreement with the observations. However, at Gulf of Suez, the mesoscale channelling effect was not well resolved by the reanalysis data.

Extreme winds at other places because of weather phenomena of different scales are also examined for the reanalysis data, including the local strong winds the Mistral in the Gulf of Lions and the Bora in the northern Adriatic Sea, the typhoons in the western North Pacific and the cyclones in the Caribbean Sea. Except for the Caribbean cyclones that are mostly of sizes smaller than the reanalysis data resolution, the other weather phenomena can actually be identified in the reanalysis data. It is a surprise that the Mistral and Bora are recognizable, given that both are classified as katabatic winds with a different mechanism from that expressed by equation (3). However, the 50 year wind is generally underestimated. For these cases, the mesoscale features are important and they will not be resolved if we downscale the background geostrophic flow directly to the micro-scale in WAsP Engineering. Downscaling by use of mesoscale models of these weather features may therefore be necessary.

The dynamical downscaling can be done in different ways. One way is to run a mesoscale model for decades; the regional climate model (REMO) from the Max Planck Institute in Hamburg, Germany, is such an example. In Larsén *et al.*,[40] we already gave some preliminary results on this, and it seems that the hydrostatic model REMO, with the resolutions of 10 km and 50 km over two domains, is sometimes problematic for the extreme wind estimation.

Another way to do the downscaling is to first identify extreme wind events from a global (or regional) reanalysis (or analysis) database, e.g. the NCEP/NCAR reanalysis data or the final analysis data (FNL) from NCEP at a resolution of 1º. In the next step, we drive a mesoscale model, e.g. Weather Research and Forecasting, for these storm episodes and calculate the extreme winds from the downscaled storms.

By using the second downscaling technique, it is of great interest to find out how well the general circulation models capture the extreme wind events in different places, e.g. the Mistral and the Bora, because first of all, they need to be identified. We leave the work of identifying further detailed characteristics of these local strong winds to a future study.

DOI: 10.1002/we

Conclusion

In this study, we have tested the method to estimate extreme winds by using the reanalysis data from the global circulation model from NCEP/NCAR. This method first calculates the geostrophic wind at sea level (G_{sl}) from the pressure, and then extrapolates G_{sl} to the wind at 10 m over a homogeneous surface with a roughness length 0.05 m, the so-called standard wind (u_{st}). Using the computer code WAsP Engineering with appropriate roughness and orography, u_{st} can be transformed to a more realistic wind for the local conditions.

The method works satisfactorily for low elevation areas such as parts of northern Europe, where the extreme winds are driven by synoptic mid-latitude lows. However, for places where the extreme winds are mesoscale phenomena, downscaling procedures using mesoscale models are needed in order to obtain more accurate extreme wind estimation.

Acknowledgements

This work is supported by Danish Research Agency grant 2104-04-0005 'Offshore wind power' and the EC 'Wind Energy Assessment Studies and Wind Engineering' (WINDENG) Training Network (contract n. HPRN-CT-2002-00215). We thank Leif Kristensen, Jake Badger and Michael Courtney for comments and suggestions. The NCEP/NCAR data are provided by the NOAA-CIRES Climate Diagnostics Center, Boulder, Colorado, from their web site at http://www.cdc.noaa.gov/.

References

1. International Electrotechnical Commission. International Standard IEC 61400-61401. *Technical Report* ISBN 2-8318-8161-7, 2007.
2. Eurocode. Eurocode 1, basis of design and actions on structure—Parts 2–4: actions on structure—wind actions. *European Committee For Standardization Technical Report*, Rue de Stassart, Brussels, 1995.
3. Kristensen L, Rathmann O, Hansen SO. Extreme winds in Denmark. *Journal of Wind Engineering and Industrial Aerodynamics* 2000; **87**: 147–166.
4. Sacré C. Extreme wind speed in France: The '99 storms and their consequences. *Journal of Wind Engineering and Industrial Aerodynamics* 2002; **90**: 1163–1171.
5. Kasperski M. A new wind zone map of Germany. *Journal of Wind Engineering and Industrial Aerodynamics* 2002; **90**: 1271–1287.
6. Mann J, Larsén XG, Jørgensen HE. Regional extreme wind climates and local winds. The one day conference on extreme winds and developments in modelling of wind storms, Cranfield University, 15 September 2004. [Online]. Available: http://www.waspengineering.dk/ExtremeAtlas/RMS4pageAbstract.pdf. (Accessed 7 January 2009)
7. Miller C. A once in 50-year wind speed map for Europe derived from mean sea level pressure measurements. *Journal of Wind Engineering and Industrial Aerodynamics* 2003; **91**: 1813–1826.
8. Kalnay E, Kanamitsu M, Kistler R, Collins W, Deaven D, Gandin L, Iredell M, Saha S, White G, Woollen J, Zhu Y, Celliah M, Ebisuzaki W, Higgins W, Janowiak J, Mo KC, Ropelewski C, Wang J, Leetmaa A, Reynolds R, Jenne R, Joseph D. The NCEP/NCAR 40-year reanalysis project. *Bulletin of the American Meteorological Society* 1996; **77**: 437–471.
9. Mann J, Ott S, Jørgensen B, Frank H . WAsP Engineering 2.0. *Technical Report Risoe-R-1356 (EN)*, Risø National Laboratory, Roskilde, Denmark, 2002. [Online]. Available: http://www.risoe.dk/rispubl/VEA/ris-r-1356.htm. (Accessed 7 January 2009)
10. Frank HP . Extreme winds over Denmark from the NCEP/NCAR reanalysis. *Technical Report Risoe-R-1238 (EN)*, Risø National Laboratory, Roskilde, Denmark, 2001. [Online]. Available: http://www.risoe.dk/rispubl/VEA/ris-r-1238.htm. (Accessed 7 January 2009)
11. Landberg L, Myllerup L, Rathmann O, Petersen EL, Jørgensen BH, Badger J, Mortensen NG. Wind resource estimation—an overview. *Wind Energy* 2003; **6**: 261–271.
12. Troen I, Petersen EL. *European Wind Atlas*. Risø National Laboratory: Roskilde, Denmark, 1989.
13. Abild J, Nielsen B. Extreme values of wind speeds in Denmark. *Technical Report M-2842*, Risø National Laboratory, Roskilde, Denmark, 1991.

DOI: 10.1002/we

14. Abild J, Mortensen NG, Landberg L. Application of the wind atlas method to extreme wind speed data. *Journal of Wind Engineering and Industrial Aerodynamics* 1992; **41**: 473–484.
15. Abild J. Application of the wind atlas method to extremes of wind climatology. *Technical Report Risoe-R-722 (EN)*, Risø National Laboratory, Roskilde, Denmark, 1994.
16. Tennekes H. Similarity relations, scaling laws and spectral dynamics. In *Atmospheric turbulence and air pollution modelling*. Nieuwstadt FTM, van Dop H, (eds). D. Reidel Publishing Company: Dordrecht, 1982; 37–68.
17. Zilitinkevich SS. Velocity profiles, the resistance law and the dissipation rate of mean flow kinetic energy in a neutrally and stably stratified planetary boundary layer. *Boundary-Layer Meteorology* 1989; **46**: 367–387.
18. Dorman JL, Sellers PJ. A global climatology of albeto, roughness length and stomatal resistance for atmospheric general circulation models as represented by the simple biosphere model (SiB). *Journal of Applied Meteorology* 1989; **28**: 833–855.
19. Kistler R, Kalnay E, Collins W, et al. The NCEP/NCAR 50-year reanalysis: Monthly means CD-ROM and documentation. *Bulletin of the American Meteorological Society* 2001; **82**: 247–267.
20. Bromwich DH, Fogt RL. Strong trends in the skill of the ERA-40 and NCEP-NCAR reanalyses in the high and midlatitudes of the southern hemisphere, 1958–2001. *Journal of Climate* 2004; **17**: 4603–4619.
21. Harris RI. The accuracy of design values predicted from extreme value analysis. *Journal of Wind Engineering and Industrial Aerodynamics* 2001; **89**: 153–164.
22. Larsén XG, Mann J. The effects of disjunct sampling and averaging time on mean maximum wind. *Journal of Wind Engineering and Industrial Aerodynamics* 2006; **94**: 581–602.
23. Watson GM, Halliday JA, Palutikoff JP, Holt T, Barthelmie RJ, Coelingh JP, Folkerts L, Van Zuylen EJ, Cleijne JW. POWER—a methodology for predicting offshore wind energy resources. *Proceedings of the 21st BWEA conference*. Cambridge, 1999.
24. Holton JR. *An Introduction to Dynamic Meteorology*. Academic Press: London, 1992.
25. Kristensen L, Jensen G. Geostrophic winds in Denmark: A preliminary study. *Technical Report Risoe-R-1145 (EN)*, Risø National Laboratory, Roskilde, Denmark, 1999.
26. Sinclair MR. Objective identification of cyclones and their circulation intensity, and climatology. *Weather and Forecasting* 1997; **12**: 595–612.
27. Benjamin SG, Miller PA. An alternative sea level pressure reduction and a statistical comparison of geostrophic wind estimations with observed surface winds. *Monthly Weather Review* 1990; **118**: 2099–2116.
28. Mohr M. Problems with the mean-sea-level pressure field over the western United States. *Monthly Weather Review* 2004; **132**: 1952–1965.
29. Pauley PM. An example of uncertainty in sea level pressure reduction. *Weather and Forecasting* 1998; **13**: 833–850.
30. Mesinger F, Treaton RE. Horizontal reduction of pressure to sea level: Comparison against the NMC's Shuell method. *Monthly Weather Review* 1995; **123**: 59–68.
31. Gumbel EJ. *Statistics of Extremes*. Columbia University Press: New York, 1958.
32. Hosking JRM. Estimation of the generalized extreme value distribution by the method of probability-weighted moments. *Technometrics* 1985; **27**: 251–261.
33. Mann J, Kristensen L, Jensen NO. Uncertainties of extreme winds, spectra and coherences. In *Bridge Aerodynamics*. Larsen, A, Esdahl, S (eds). Balkema: Rotterdam, 1998.
34. Simiu E, Heckert NA. Extreme wind distribution tails: A "peak over threshold" approach. *Journal of Structural Engineering* 1996; **122**: 539–547.
35. Holmes JD, Moriarty WW. Application of the generalized pareto distribution to extreme value analysis in wind engineering. *Journal of Wind Engineering and Industrial Aerodynamics* 1999; **83**: 1–10.
36. Palutikof JP, Brabson BB, Lister DH, Adcock ST. A review of methods to calculate extreme wind speeds. *Meteorological Applications* 1999; **6**: 119–132.
37. Cook NJ, Harris RI, Whiting R. Extreme wind speeds in mixed climates revisited. *Journal of Wind Engineering and Industrial Aerodynamics* 2003; **91**: 403–422.
38. Badger J, Giebel G, Larsén XG, Nielsen TS, Nielsen H, Madsen H, Tøfting J . Report on the use of stability parameters and mesoscale modelling in short-term prediction. *Technical Report Risø-R-1614 (EN)*, Risø National Laboratory, Roskilde, Denmark, 2007.
39. Ott S . Extreme winds in the western North Pacific. *Technical Report Risoe-R-1544 (EN)*, Risø National Laboratory, Roskilde, Denmark, 2005.
40. Larsén XG, Mann J, Göttel H, Jacob D. Wind climate and extreme winds from the regional climate model REMO. In *Scientific Proceedings of the European Wind Energy Conference and Exhibition*, Brussels, 2008; 58–62.

DOI: 10.1002/we